

Doppler imaging of stellar surface structure

XI. The super starspots on the K0 giant HD 12545: larger than the entire Sun

K.G. Strassmeier*

Institut für Astronomie, Universität Wien, Türkenschanzstrasse 17, A-1180 Wien, Austria (strassmeier@astro.univie.ac.at)

Received 22 March 1999 / Accepted 4 May 1999

Abstract. The active K0 giant HD 12545 is the star with the largest starspots ever observed. We report a record light-curve amplitude of 0.^m63 in V and 0.^m17 in V-I in January 1998. At the same time, HD 12545 was at its brightest magnitude since the discovery of its light variability in 1985. We present the first Doppler image of HD 12545 from observations during this state of high-amplitude light variability and find that the star exhibits one cool high-latitude spot of gigantic dimensions (\approx 12×20 solar radii, i.e. 60 times the extension of the largest sunspot group or 10,000 times larger areal coverage). Furthermore, our map shows one smaller cool spot and one equatorial warm (bright) spot. The warm spot is situated approximately 180° from the large cool spot in the opposite hemisphere and is the cause of the exceptionally large light-curve amplitude and the stellar brightening. Within our model, no light-curve nor a reasonable lineprofile solution with only cool spots was possible. Surprisingly, the fact that HD 12545 is brighter at a time of high spot activity is in agreement with solar analogy. Our data also allow to refine the orbital elements of HD 12545 and we use the Hipparcos parallax to determine absolute astrophysical quantities for this rapidly rotating K giant.

Key words: stars: activity – stars: imaging – stars: individual: HD 12545 – stars: late-type – stars: starspots

1. Introduction

The RS CVn binary HD 12545 = XX Tri (K0III, $P_{\rm orb} \approx P_{\rm rot} \approx$ 24 days) is among the most active stars of the RS CVn class exhibiting strong UV emission-line fluxes up to 400 times the solar values (Bopp et al. 1993), Ca II H & K emission-line intensities 2–3 times that of the nearby continuum (Bidelman 1985, Strassmeier et al. 1990), and strong coronal X-ray emission (Dempsey et al. 1993). But most noteworthy for optical observers is its huge photometric variability with an amplitude of $0^{\rm m}_{..}60$ in V in late 1990 (Nolthenius 1991), and again a record amplitude of $0^{\rm m}_{..}63$ during the observations for this paper in 1997/98. These

amplitudes are the largest amplitudes ever recorded for a post-main-sequence star (the absolute record holder is the weak-lined T Tauri star V410 Tau with 0. 65 in 1994/95; Strassmeier et al. 1997a) and are commonly attributed to rotational modulation of an asymmetrically spotted stellar surface having spots cooler than the photosphere. Such an assumption seems to be appropriate due to the analog of sunspots, despite that the Sun's photometric V-band amplitude is typically only 0. 001.

Ten years of photometry of HD 12545 from various sources indicated a systematic waxing and waning of the light-curve amplitude reminiscent of a sunspot cycle with a yet unpredictable periodicity (Strassmeier et al. 1997a). Spot modeling of rotationally modulated light and color curves by two independent groups (Strassmeier & Oláh 1992 and Hampton et al. 1996) gave conflicting surface spot distributions. The main reason for these discrepancies is that photometry alone can not constrain a spot's latitude, nor can it reliably recover a surface spot distribution when the inclination of the rotation axis and the level of unspotted brightness are unknown. Just recently, Vogt et al. (1999) presented a comparison of Doppler images and spot distributions from light-curve modeling of the RS CVn binary HR 1099 and showed that simple two-spot model solutions are often misleading and nonunique. Clearly, spot distributions determined from photometry alone are model dependent.

These shortcomings are not present in Doppler imaging, which uses the deformations of rotationally-broadened line profiles to recover the stellar surface temperature distribution (e.g. Rice 1996, and previous papers in this series). Together with simultaneous multi-color photometry, which is used to define the absolute and relative continuum flux, it is possible to obtain accurate physical spot quantities and compare these values with the Sun and other stars.

2. Observations

The spectroscopic observations were obtained at Kitt Peak National Observatory (KPNO) with the 0.9-m coudé feed telescope during 24 consecutive nights in December and January 1997/98. The 800^2 TI-5 CCD detector was employed together with grating A, camera 5, the long collimator, and a 280- μ m slit to give a resolving power of 38,000 at 6420 Å, or 0.19 Å as judged from the FWHM of unblended Th-Ar comparison-lamp lines.

^{*} Visiting Astronomer, Kitt Peak National Observatory, operated by the Association of Universities for Research in Astronomy, Inc. under contract with the National Science Foundation

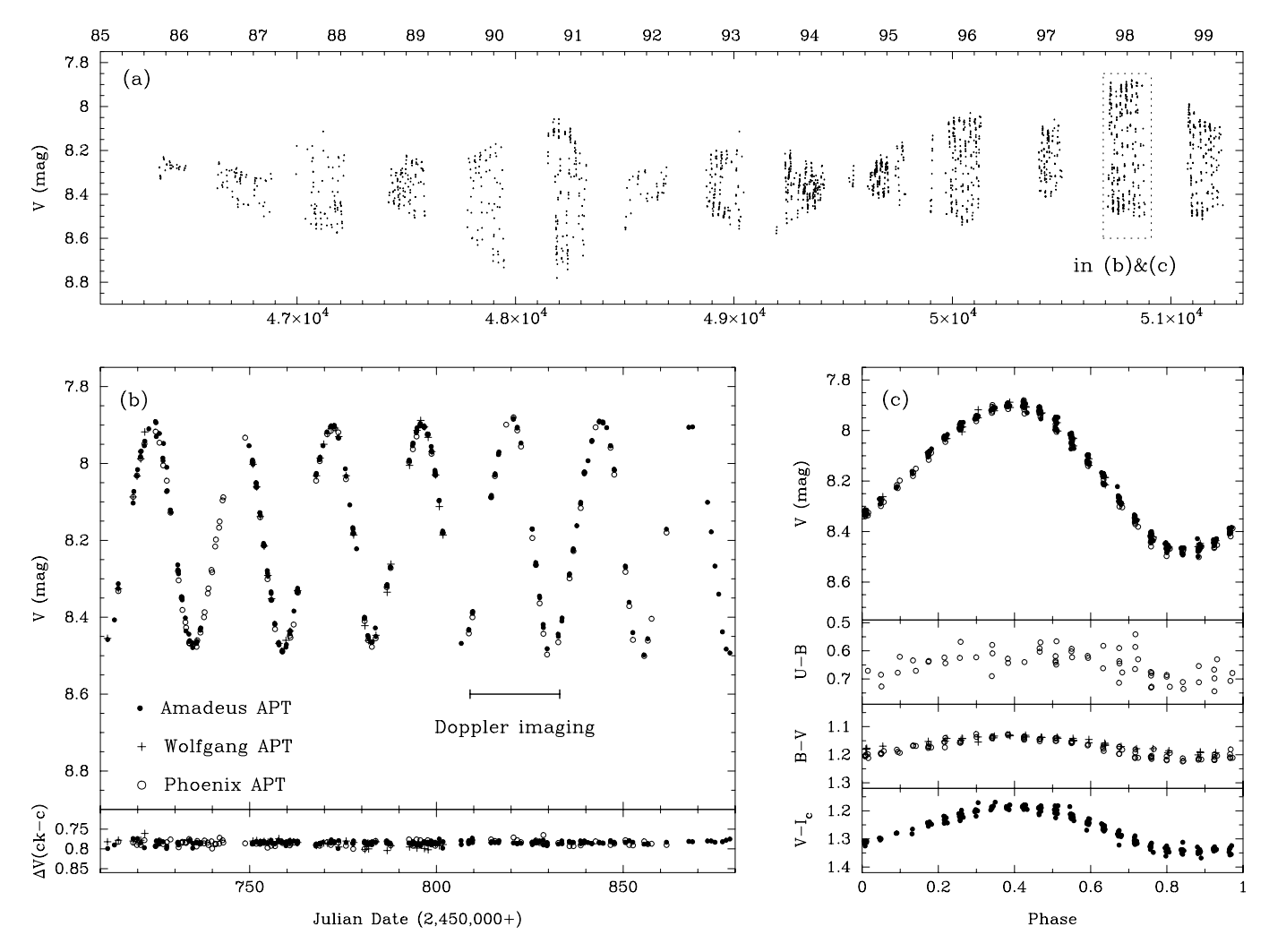


Fig. 1a–c. Photometry of HD 12545. **a** The long-term V light curve from 1985 through 1999. Data prior to 1996.5 were taken from Strassmeier et al. (1997a) and literature cited therein, data after 1996.5 are from the present paper. Notice that the star was at its brightest level ever in January 1998 (JD 2,450,820). The x-axis is given as JD minus 2,400,000 days. Years minus 1900 are indicated as well. **b** Seasonal 1997/98 V data (the lower panel shows the differential check minus comparison magnitudes). The time of our Doppler-imaging observations at KPNO is marked and coincided with the time of the star's highest brightness. **c** The same data as in panel **b** but phased with our ephemeris in Eq. (1). Notice that the scatter in the light and color curves is mostly due to intrinsic changes from one rotation to the next and not due to instrumental scatter (however, U-B has about 10 times higher scatter than V). All color variations are in phase with the V-light curve, suggesting a common cause.

The full wavelength range was 80 Å and each spectrum was exposed for 3600 sec, except the last two which were exposed for 2700 sec. The analog-to-digital units in the continuum correspond to signal-to-noise ratios of around 250:1. Numerous nightly flat fields were co-added and used to remove the pixel-to-pixel variations in the stellar spectra. The TI-5 CCD shows no signs of fringing around 6400 Å and no attempts were made to correct for it other than the standard flat-field division. Continuum fitting with a very low-order polynomial was sufficient to find an excellent continuum solution.

Continuous Johnson UBV, $V(I)_C$, and Strömgren by photometry of HD 12545 is being obtained with three automatic photoelectric telescopes (APTs) at Fairborn Observatory in southern Arizona since late 1996. With Wolfgang-Amadeus, the two 0.75-m twin Vienna Observatory APTs (Strassmeier et al. 1997b), we obtained $V(I)_C$ and by photometry, and with the

Phoenix-10 0.25-m APT (Seeds 1995), we obtained UBV photometry. All measures were made differentially with respect to HD 12478 (V=7...710, V- I_c =1...38; Strassmeier & Oláh 1992) as the comparison star and SAO 55178 as the check star. Three measures in VI_C and by were taken per night by Wolfgang-Amadeus and one in UBV by the Phoenix-10. One observation consisted of three ten-second (30-sec in by) integrations on the variable, four integrations on the comparison star, two integrations on the check star, and two integrations on the sky. A 30" diaphragm was used with Wolfgang-Amadeus and a 60" diaphragm on the Phoenix-10. The standard error of a nightly mean from the overall seasonal mean was for Wolfgang 0...003 in by, for Amadeus 0...004 in V and 0...006 in I_c , and for the Phoenix-10 0...09 in BV and 0...02 in U. For further details we refer to Strassmeier et al. (1997a, 1997b).

3. Astrophysical parameters of HD 12545

All previous investigations of this star were hampered by the fact that no trigonometric parallax was available. Distance estimates had therefore an unacceptable large range of 77–340 pc, depending on the adopted spectral classification (see the discussion in Bopp et al. 1993). Here, we use the new Hipparcos parallax to redetermine the fundamental astrophysical parameters of HD 12545.

3.1. Distance, effective temperature, luminosity, gravity, and mass

The Hipparcos satellite (ESA 1997) measured a parallax of 5.08 ± 1.1 milli-arcsec and finally fixed the distance of HD 12545 to 197^{+54}_{-35} pc. With the brightest, i.e. presumably unspotted, V magnitude of 7.º 875 observed in early 1998 (Fig. 1a), the absolute visual magnitude of HD 12545 is $M_{\rm V}=+1^{\rm m}20^{+0.42}_{-0.53}$. However, as we will show later in Sect. 4.4, the brightest magnitude is affected by a large warm spot and is probably too bright for the true unspotted magnitude. The estimated difference is approximately 0.1 and, if taken into account, would change the absolute brightness only by $1/4-\sigma$ because its error bars are dominated by the uncertainty of the parallax. In any case, the absolute brightness of about +1^m2 confirms the class III giant luminosity classification from the optical spectrum (Strassmeier & Oláh 1992, Bopp et al. 1993). Interstellar absorption was taken into account with 0.1 per 100 pc. Such a value is in agreement with the observed B-V color from Hipparcos and that of a K0III star from the tables of, e.g. Gray (1992), which would suggest E(B-V) \approx 0.0000 or $A_V \approx$ 0.00000 3 \pm 0.1, in accordance with our adopted value of 0.^m2. We note that a B-V excess of 0.11 from our new BV photometry and the K0III classification would result in a slightly higher value of $A_V \approx 0^{\text{m}}35$ instead of 0.2. However, even the bluest B-V color ever observed is likely affected by the heavy spottedness of HD 12545 and is not recommended to be used for spectral classification.

Our gravity estimate relies on the spectrum synthesis of the pressure sensitive wings of the strong Ca I 6439-Å line. There are several blends in the wings of this line, e.g. Eu II and Y I, whose strengths and chemical abundances are not known. Consequently, our $\log g$ determination is uncertain but must be in the 2.5–3.0 range, in agreement with the canonical values for a K0 giant (e.g. Gray 1992).

The dereddened B-V color of 1 $^{\rm m}$ 04 indicates $T_{\rm eff}$ of 4750 K according to the tables of Gray (1992) and Flower (1996). With a bolometric correction of -0.437 (Flower 1996), the bolometric magnitude of HD 12545 is +0.765 and, with an absolute magnitude for the Sun of $M_{\rm bol,\odot}=+4.764$ (Schmidt-Kaler 1982), the luminosity must be approximately 35_{-11}^{+22} L $_{\odot}$. The position of HD 12545 relative to the evolutionary tracks of Schaller et al. (1992) for solar metallicity suggests then a mass of $1.8_{-0.2}^{+0.3}$ M $_{\odot}$ (Fig. 2). The fact that a strong lithium line was detected in the spectrum of HD 12545 ($\log n({\rm Li}) \approx 1.7$; Strassmeier & Oláh 1992, Bopp et al. 1993) favors the picture that the star is on the red-giant branch and not yet in the helium-core burning phase.

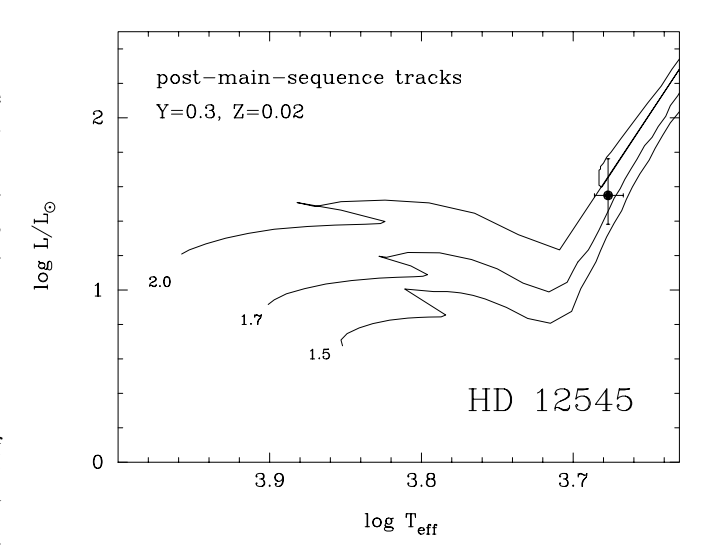


Fig. 2. The observed position of HD 12545 (dot) in the H-R diagram. Shown are post-main-sequence tracks for 2.0, 1.7, and 1.5 solar masses from Schaller et al. (1992) that suggest a mass for HD 12545 of around 1.8 M_{\odot} .

3.2. Rotational velocity and stellar radius

Doppler imaging allows a more accurate determination of the projected rotational velocity, $v \sin i$, than any other technique. This is because the line asymmetries due to the spots are explicitely modeled. A wrong $v \sin i$ would produce a pronounced, artificial band encircling the star being either bright or dark depending whether the adopted $v \sin i$ was too large or too small, respectively (see, e.g., Vogt et al. 1987). Avoiding such a feature yields our value for the projected rotational velocity of $20.8 \pm 0.5 \, \mathrm{km \, s^{-1}}$. Together with the rotation period of $24.0 \, \mathrm{days}$ it results in a minimum radius of $R \sin i = 9.9 \pm 0.2 \, R_{\odot}$. If $i \approx 60 \pm 10^{\circ}$ is the correct inclination, as indicated later in Fig. 4, the stellar radius is $\approx 11.4^{+2.0}_{-0.8} \, R_{\odot}$. The unprojected equatorial rotational velocity, $v_{\rm eq}$, would then be $24.0 \, \mathrm{km \, s^{-1}}$.

3.3. Radial velocities, orbital period, and space kinematics

Bopp et al. (1993) presented a first zero-eccentricity SB1 orbit and found a period of 23.9729±0.0022 days from 44 radial velocities taken between 1985 and 1992. We add our 14 velocities from Table 1 to refine the orbital elements. The adopted velocities for our cross-correlation stars were 3.2 km s⁻¹ for β Gem (K0III), -14.5 km s^{-1} for α Ari (K2III), and $+54.3 \text{ km s}^{-1}$ for HR 8551 (K0III-IV) (Scarfe et al. 1990). No systematic velocity differences were evident, but two of the velocities from Bopp et al. (1993) were given zero weight. The radial velocity curve is plotted in Fig. 3 and the revised elements are: $P_{\rm orb} = 23.96924 \pm 0.00092$ days, $\gamma = -26.35 \pm 0.18$ ${\rm km}\,{\rm s}^{-1},\,e=0$ (adopted), $K=15.9\pm0.2~{\rm km}\,{\rm s}^{-1},\,a\sin i=$ $5.24 \pm 0.07 \times 10^6$ km, and $f(M) = 0.0100 \pm 0.0004$. The standard error of an observation of unit weight was 1.23 km s^{-1} , slightly higher than the average internal error of a single observation (Column $\sigma_{\rm vr}$ in Table 1). We attribute this to the fact that the spots cause systematic line asymmetries and thus asym-

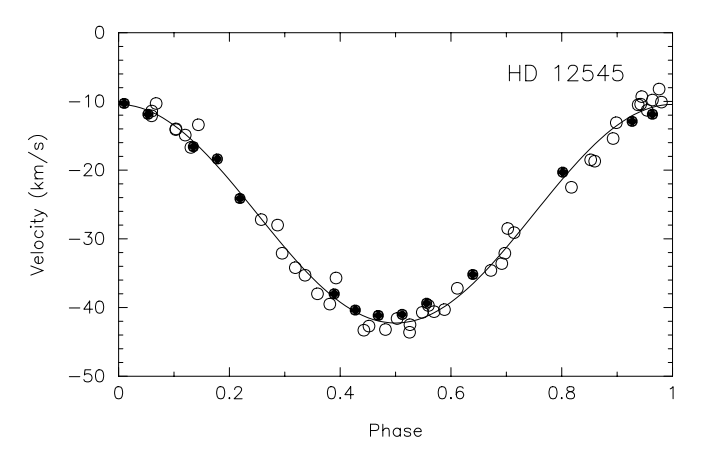


Fig. 3. Radial velocity curve and orbit. The open circles are from Bopp et al. (1993) and the full circles are from the present paper. Zero weight was given to the two deviant points at phase 0.40 and 0.15.

Table 1. Spectroscopic observing log and radial velocities

HJD	Phase	$v_{ m r}$	$\sigma_{ m vr}$	O-C	Reference
(24+)	(Eq. 1)	(k	${\rm cms^{-1}}$)	star
50809.611	0.964	-12.1	1.5	-1.0	α Ari
50810.721	0.010	-10.3	1.2	+0.2	β Gem
50811.750	0.053	-12.1	1.4	-0.5	α Ari
50813.714	0.135	-16.6	1.7	-0.8	β Gem
50814.754	0.178	-18.6	0.6	+1.0	α Ari
50815.732	0.219	-24.3	0.8	-0.8	α Ari
50819.811	0.389	-38.2	0.6	+0.5	α Ari
50820.721	0.427	-40.4	0.5	+0.3	β Gem
50821.717	0.469	-41.1	0.5	+0.8	β Gem
50822.750	0.512	-41.0	0.7	+1.2	β Gem
50823.809	0.556	-39.4	0.7	+1.9	β Gem
50825.807	0.639	-35.2	0.7	+1.3	β Gem
50829.699	0.802	-20.3	0.7	+0.9	HR 8551
50832.703	0.927	-12.9	0.6	-0.8	HR 8551

metric cross-correlation functions. The radial velocities along with the observed minus computed velocities, O-C, are listed in Table 1.

Throughout this paper phase is always computed from a time of maximum positive radial velocity with the revised orbital period,

$$HJD = 2,447,814.325 + E \times 23.96924$$
. (1)

Together with the distance and proper motions from Hipparcos, the revised space velocities of HD 12545 relative to the Sun in a right-handed coordinate system are (U,V,W)=(+55 ± 10 , +9 $^{+6}_{-4}$, -16 $^{+5}_{-9}$) km s $^{-1}$. The space velocity vector, $S=\sqrt{U^2+V^2+W^2}$, is then 58 km s $^{-1}$, typical for old disk and halo stars according to the criteria of Eggen (1969). The nominal age from the tracks of Schaller et al. (1992) is 1.8×10^9 yr.

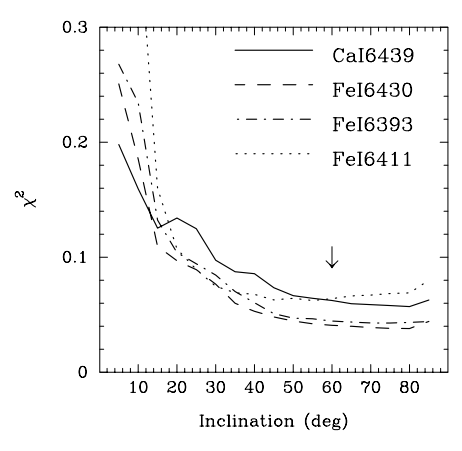


Fig. 4. The dependence of the normalized goodness of fit (χ^2) on the adopted stellar inclination angle as discussed in Sect. 4.3. The different line styles are for the different spectral regions.

4. Doppler imaging

4.1. The TempMap code

As in previous papers in this series, all maps were generated with the Doppler-imaging code *TempMap* of Rice et al. (1989). This code was originally developed for use with chemicalabundance inhomogeneities of Ap stars but was successively adapted for temperature recovery (Rice 1996; see Rice & Strassmeier 1998 for a brief update). In this paper, we chose a Maximum-Entropy regularization. A grid of 10 model atmospheres with temperatures between 3500 K and 6000 K and $\log q = 2.5$ were taken from the ATLAS-9 CDs (Kurucz 1993). For temperatures not within ± 10 K of one of the tabulated input atmospheres, we interpolate between them. Due to the narrow spectral lines of HD 12545, blending of the main mapping lines must be considered very carefully. We emphasize that TempMap uses all spectral line profiles in a particular spectral region for the "inversion", i.e. the main mapping line plus the blends, and thus even considers the (subtle) mainprofile changes due to the spot-induced periodic changes of the blend-line profiles. The number of blends vary from spectral region to spectral region and were tabulated in previous papers in this series (e.g. Strassmeier 1997). We make use of six line regions centered at the following main spectral lines (the number in parenthesis is the number of included blends): Ca I 6439.075 Å (4), Fe I 6430.844 Å (8), Fe I 6421.349 Å (6), Fe I 6419.942 Å (7), Fe i 6411.649 Å (8), and Fe i 6393.602 Å (4). The adopted $\log gf$ values and lower excitation potentials (in eV) are +0.47/2.53, -2.10/2.18, -2.10/2.28, -0.24/4.73, -0.60/3.65, and -1.62/2.43, respectively.

4.2. Doppler imaging at low spatial resolution

The 24-day rotation period of HD 12545, together with the need to cover all rotational phases within a single stellar rotation, makes access to high-resolution spectrographs at large telescopes practically impossible. With the current resolving power of $\lambda/\Delta\lambda$ =38,000 (i.e. 0.19 Å at 6430 Å) and a full width

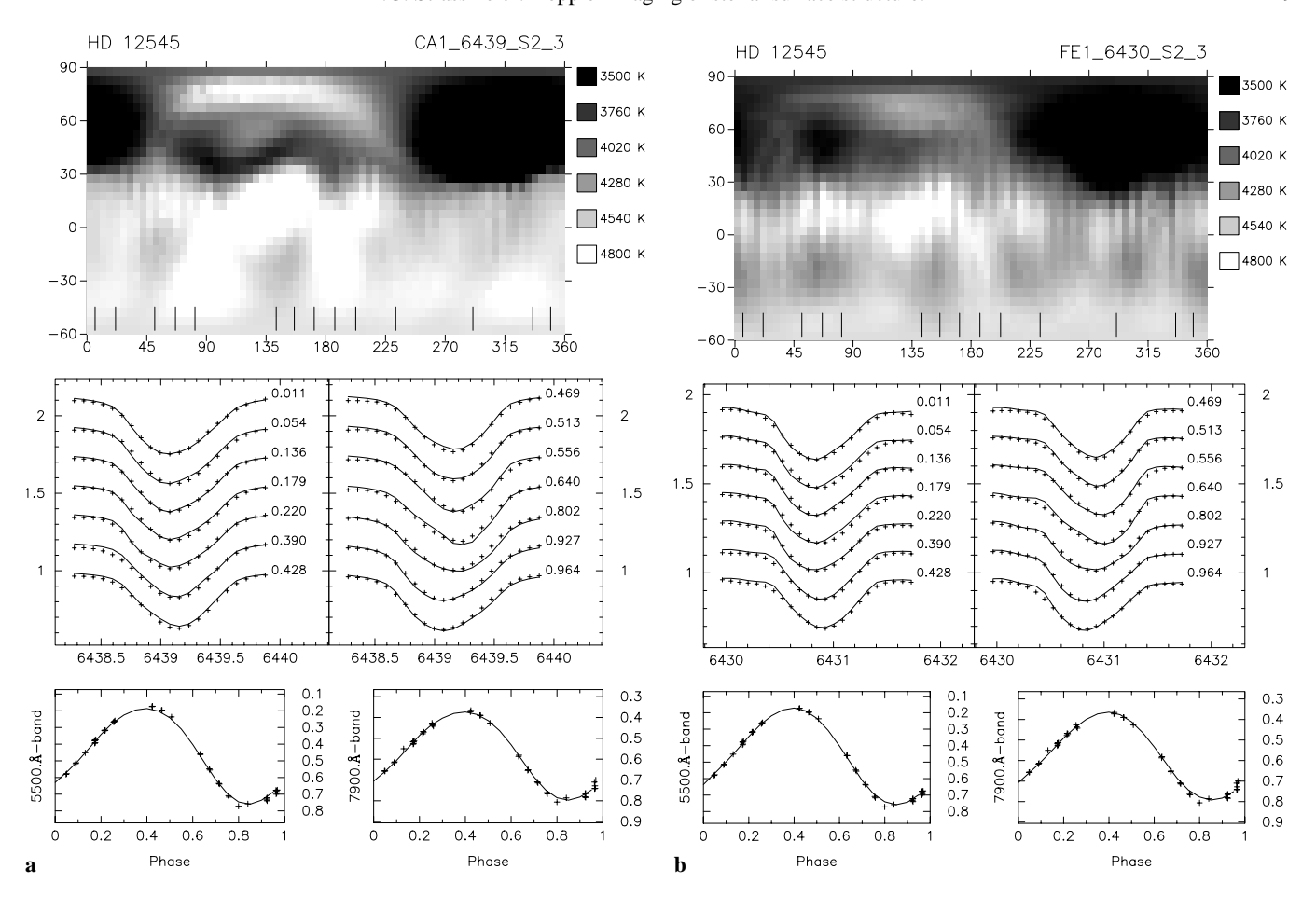


Fig. 5a–f. Doppler images of HD 12545 for six different spectral regions. **a** Ca I 6439 Å, **b** Fe I 6430 Å, **c** Fe I 6411 Å, **d** Fe I 6393 Å, **e** Fe I 6421 Å, and **f** Fe I 6419 Å, All maps were obtained with Johnson B (4340 Å), V (5500 Å) and Cousins I_C (7900 Å) photometry, but only the VI maps are shown. The thick marks in the maps indicate the phase coverage.

of the lines at continuum level of $2 (\lambda/c) v \sin i \approx 0.87 \text{ Å}$, we have just 4.5 resolution elements across the stellar disk. According to the simulations of Piskunov & Wehlau (1990) this is the limit for a detailed recovery and their test inversions with artificial data still showed a fully correct recovery of the input image when five resolution elements were available. However, surface detail much smaller than a resolution element is being lost and the reconstructed detail depends on latitude (and stellar inclination) and on the phase coverage. Usually, low-latitude features are less reliable than high-latitude features. A similar conclusion was reached by Strassmeier & Rice (1998) from their test inversions with $v \sin i = 17.5 \text{ km s}^{-1}$ to simulate the line profiles of the G2-dwarf EK Dra, while Hatzes (1993) concluded that Doppler imaging should be capable of recovering spots on stars rotating as slowly as 15 km s^{-1} . HD 12545 shows a very large light-curve amplitude and thus presumably very large spots that, in turn, cause large spectral-line deformations, which makes the recovery more reliable. Phase smearing due to the one hour integration time amounts to just 0.0017, or less than 1° at the stellar central meridian, and is negligible. The intrinsic (thermal) width of our mapping lines is always much smaller than the width of the instrumental profile and also does not further decrease the

spatial resolution. Nevertheless, we caution not to overinterpret the details in the images (better data are always better).

4.3. The inclination of the stellar rotation axis

The revised mass function of 0.0100 ± 0.0004 , together with the primary mass of $1.8^{+0.3}_{-0.2}$ M_{\odot}, suggests an upper limit for the inclination angle of $78^{\circ}\pm1^{\circ}$. Above that inclination, we would see an eclipse because then $a \cos i < R_1 + R_2$. The very small mass function suggests a low-mass secondary star with masses of $0.37~{\rm M}_{\odot}$ for $i=78^{\circ}$ and $1.02~{\rm M}_{\odot}$ for $i=25^{\circ}$. Because we do not see the secondary spectrum in red, nor blue or ultraviolet (Bopp et al. 1993) wavelengths, the secondary must be always fainter by at least $\approx 2^{\text{m}}$ 5. This excludes all subgiants hotter than ≈K2 and all stars hotter than late-F. Thus, the mass ratio primary/secondary must be larger than approximately 1.5, which sets a lower limit for the inclination to 25°. However, at this inclination the K giant would already overflow its Roche lobe and should show pronounced spectroscopic signs, e.g. systematic radial-velocity shifts in high-excitation chromospheric and transition-region line profiles, which it does not. It is thus likely that the lower limit of the inclination is more around $35-40^{\circ}$.

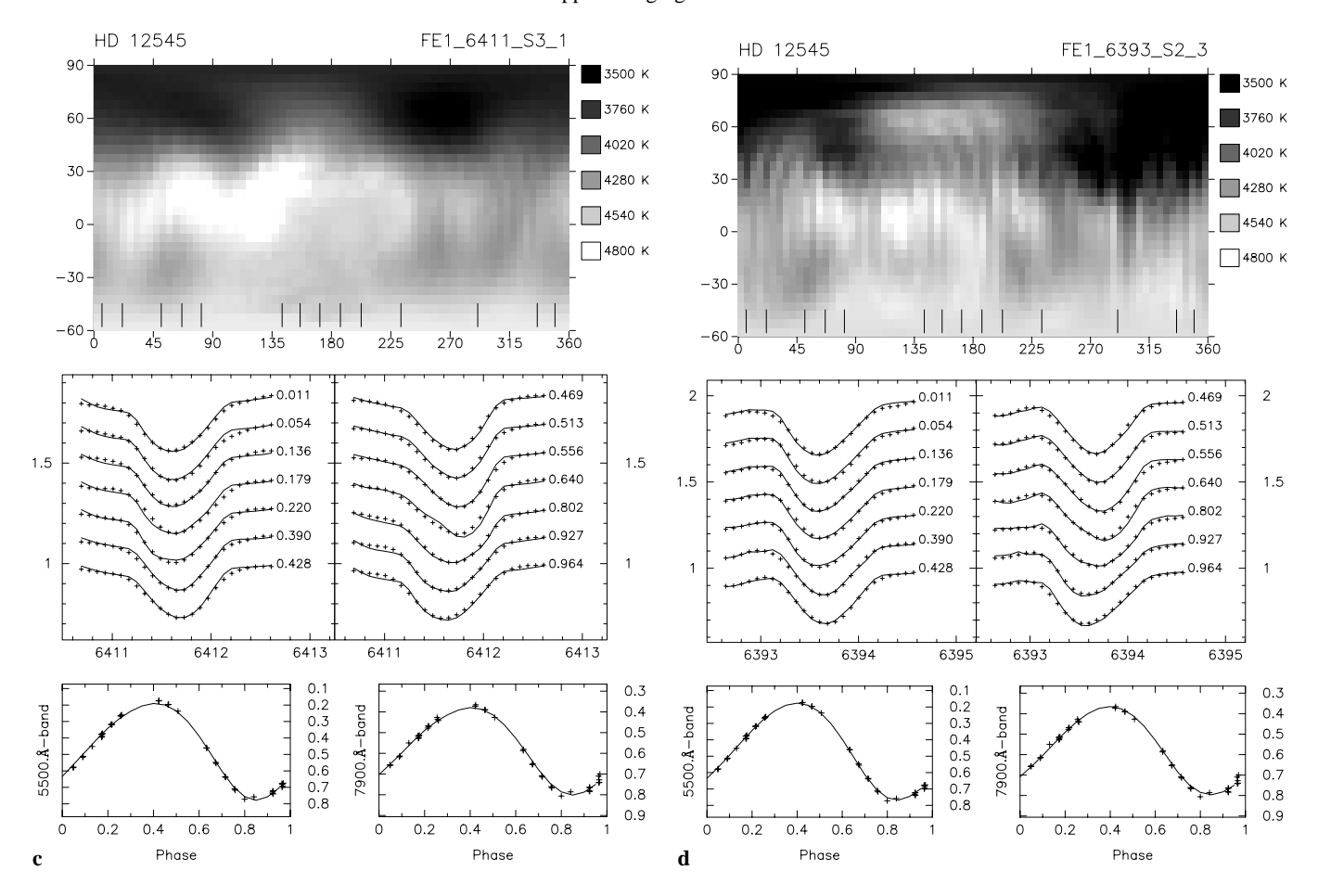


Fig. 5a-f. (continued)

We tried inclination angles between 5° and 85° for the line profile inversion and found overal the largest reduction in the sum of the squares of the residuals (at maximized entropy) when inclinations between $50\text{--}80^{\circ}$ were used (Fig. 4). Finally, we adopt $i \approx 60^{\circ}$ as the most consistent inclination from the fits of four spectral regions and above considerations. The most likely secondary star is then a $\approx 0.4~\text{M}_{\odot}$ red dwarf star of spectral type M2. Note that our conclusions would not change significantly if the maps were reconstructed with inclinations of 50° or 70° .

4.4. Results

Figs. 5a–f show the Doppler images from the six available spectral regions along with the achieved line-profile and light-curve fits. The best χ^2 -level from profiles and light curves combined is around 0.06, thus slightly worse than what we usually achieve, e.g., for the stars in previous papers in this series (e.g. Strassmeier & Rice 1998). We attribute this to two effects; first – and most important – the increased influence of uncertainties of the atomic line parameters, the line synthesis, and the external errors of our spectra with the small rotational broadening of HD 12545 and, second, a variability time scale on the stellar surface that seems to be shorter than the rotational period of 24 days. The first effect is detectable by inconsistencies in the maps from

spectral region to spectral regions. While four of the six regions agree very well, two maps (Fe I 6419 Å and 6421 Å) show some discrepancies concerning the recovered spot area, i.e. primarily the spot contrast. Both line regions turn out to be very complex blends of at least ten lines within two Ångströms including temperature sensitive vanadium and titanium lines with more than uncertain transition probabilities (see, e.g., the VALD database compiled by Piskunov et al. 1995). Disentangling the individual blend's line strengths at the atmospheric conditions of HD 12545 is therefore not straightforward and we decided to exclude these two maps from the average map but plot them in Figs. 5e and 5f for comparison purpose.

The second effect is more subtle and is primarily indicated by the small seasonal light-curve variations visible in Fig. 1b rather than by the line profiles or the reconstruction process itself. Any current Doppler-imaging code must assume that surface features remain stable during the time of the observations. From the seasonal light-curve changes and the less-than-perfect χ^2 -level of our line-profile fits, we estimate that the amount of spot variations during one stellar rotation is still less than or comparable to the surface resolution of our spectra. It is thus unlikely that spurious surface features larger than $10-20^\circ$ were introduced into our maps but the effect is that phase smearing due to a variable feature may have found its way into the data.

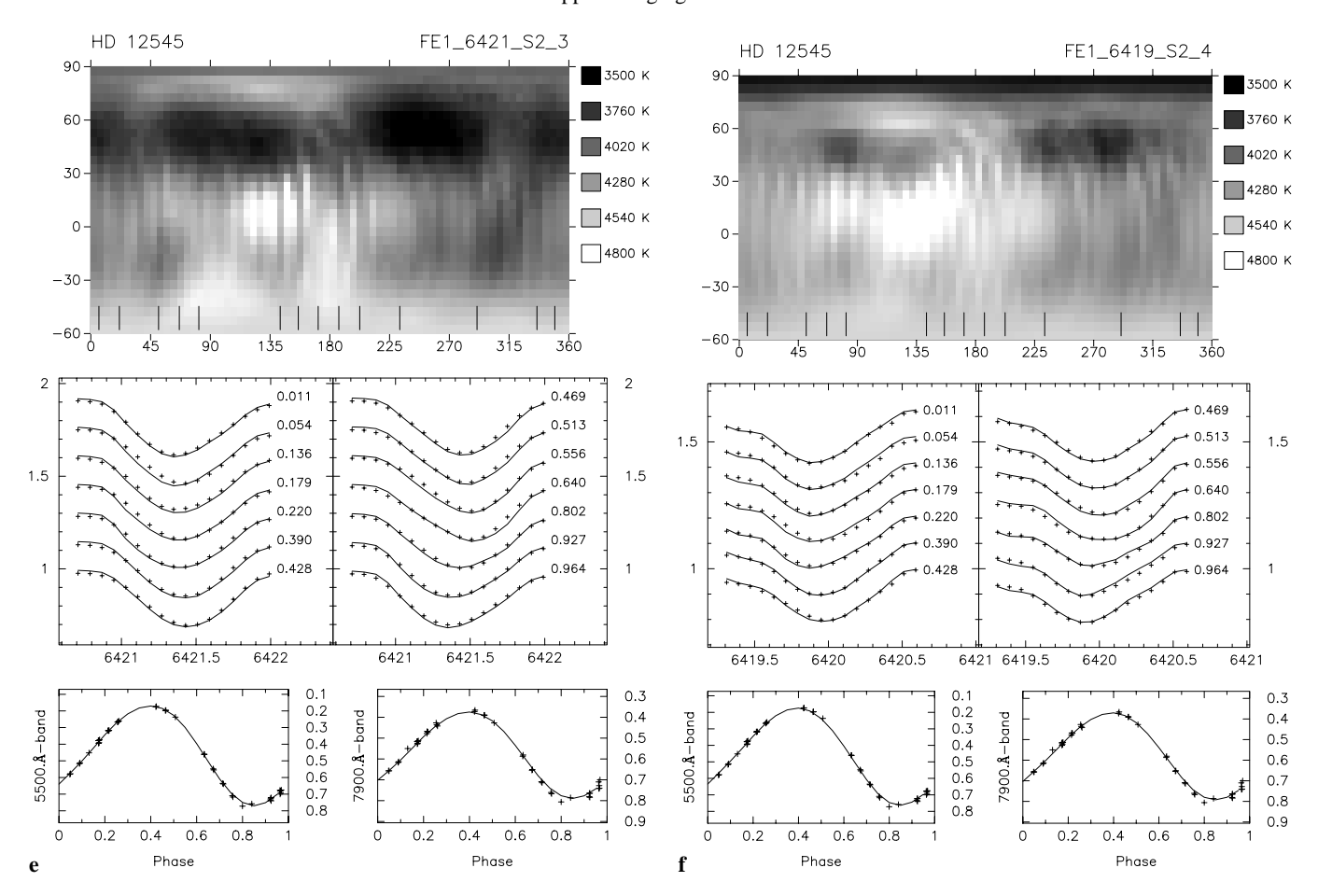


Fig. 5a-f. (continued)

However, we do not consider this a detectable effect from our data.

Besides this superspot, we reconstruct a second, but much smaller, cool spot at a longitude of $\ell \approx 90^\circ$, a latitude of $b \approx 50^\circ$ and with an area of 2.3% (at T=4000 K), as well as an equatorial warm spot (or a conglomerate of several smaller spots) around $\ell \approx 90-135^\circ$ and with an area of 3.5%. The warm feature appears on the adjacent hemisphere of the big cool spot and "south" of the smaller cool spot and, if thought about in terms of opposite polarity of the underlying magnetic field for cool and hot features, possibly indicates violent interactions that could be the reason for the short variability time scale. The sys-

tematically changing maximum brightness 1997/98 to 1998/99, shown in Fig. 1a, along with a nearly constant minimum brightness indicates that the warm feature is the cause of the light curve changes. The warm spot's recovered temperature is at most 350±20 K above the effective photospheric temperature (see the temperature profiles later in Fig. 8) and is constrained by both the line profiles and the BVI-photometry. Its size and temperature, however, is different in the maps from the different spectral lines but is recovered even when no photometry is used for the inversion. We consider this feature to be reliable and needed by the data because, first, the light and color curves can not be fitted at all (simultaneous with and without the line profiles) if we restrict spots to $T \leq T_{\rm eff}$, nor can the line profiles be consistently fitted to a comparable χ^2 -level if the photometry is completely excluded from the inversion. Note that the band of weak spots along a latitude of approximately -30° is due to the mirroring effect from the strong high-latitude features, a well-known shortcoming of Doppler imaging, and is purely artificial.

Figs. 6 and 7 show the average map from Ca_I 6439, Fe_I 6430, Fe_I 6411 and Fe_I 6393 Å, and the standard deviation map in mercator projection and pole-on projection, respectively. The pole-on projection style emphasizes surface detail at or near the visible pole as opposite to the Mercator projections which

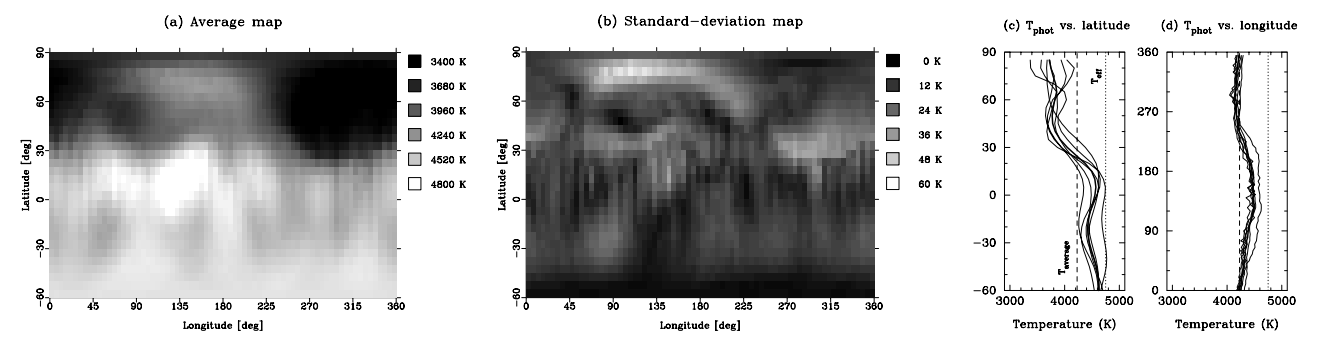


Fig. 6a–d. Mercator views of HD 12545. **a** Weighted average map in mercator projection. The maps from Fe I 6419 Å and 6421 Å gave slightly discordant results and were not included in the average map. **b** Standard-deviation map. **c**, **d** The binned temperature distributions as a function of stellar latitude and longitude for all individual maps, respectively. The dotted line shows the effective temperature from the photometric calibration, the dashed line the average surface temperature, and the thick lines show the distribution from the average map.

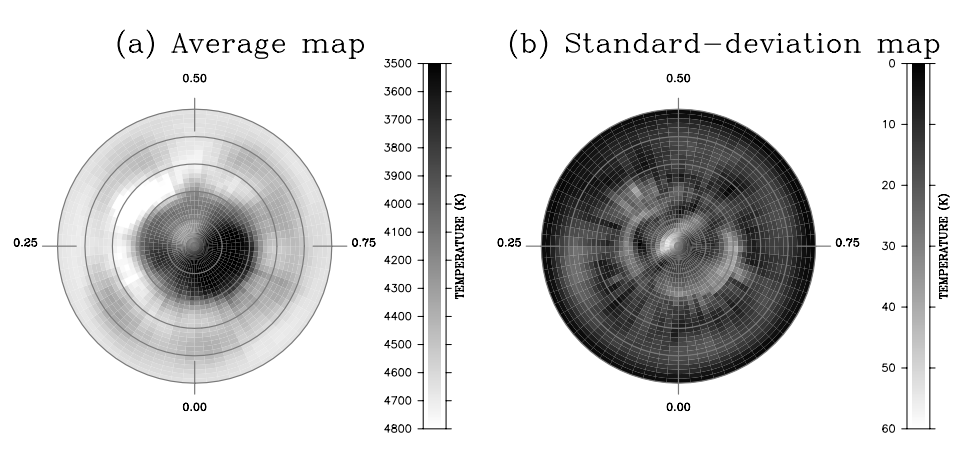


Fig. 7a and b. Pole-on views of HD 12545. a Weighted average map in pole-on view from latitude -60° (circles indicate latitudes in steps of 30°). b The standard-deviation map. As in Fig. 6b, dark areas correspond to small deviations (black=0K, white=60K), i.e the darker the grey scale the better the agreement between the individual maps.

emphasize the equatorial regions. Finally, Fig. 8 is a plot of the average map in a more realistic spherical projection. It also shows the temperature profiles along longitudinal and latitudinal cuts through the large cool spot at $\ell,b=315^\circ,+60^\circ$ and the warm spot at $\ell,b=135^\circ,+15^\circ,$ respectively.

5. Discussion and conclusions

Our observations of HD 12545 in 1997/98 caught this spotted star in its, so far, most active state. The light and color curves had a full V amplitude of 0. 63, a V-I amplitude of 0. 17, and B-V and U-B amplitudes of 0.10, respectively. At the same time, the star was at its brightest magnitude ever, 15% brighter than the previously detected high (see Fig. 1). Unexpected for a very active K0 giant, this indicates some solar analogy because the Sun also appears brighter during sunspot maximum due to an increased facular component. Dorren & Guinan (1990) observed a similar correlation for the RS CVn star HR 1099 and suggested that the long-term light variation is produced by competition between the blocking effect of the cool starspots and enhancement from white-light faculae. If true, and solar analogy applies, the U-brightness should increase with respect to the B-brightness during times when white-light faculae are visible on the stellar disk, i.e. during light-curve maximum, and the U-B index should appear bluer. Fig. 1c shows that this is indeed the case.

The observational phase of the warm spot coincides approximately with the region of the sub-stellar point, that is the part on the K giant facing the secondary star. Could the warm feature be the hot spot of the inner Lagrangian point due to ongoing mass transfer? If the inclination of 60° is approximately right (within deviations of -20° and $+40^{\circ}$), then HD 12545 is significantly far from filling its Roche lobe and appears practically spherical; its radius of 11.4 R_{\odot} is barely 50% of the critical radius and the secondary star is over four times less massive and almost exactly four stellar radii away from the primary. We also do not see systematic blue nor red shifts of high-excitation emission lines or of photospheric absorption lines in excess of $3-4 \text{ km s}^{-1}$ that would be expected due to the mass stream between the stars. Furthermore, the observed annual variations of the light-curve maximum suggests a time-variable phenomenon while a hot spot due to mass transfer should be a relatively stable phenomenon and brighten the system continuously. We can thus safely conclude that the warm feature must be due to solar-type plage or facular activity.

Because the light-curve amplitude of HD 12545 remained around 0. or V throughout the entire observing season, we estimate that the lifetime of both the warm and the large cool surface feature is at least as long, roughly 220 days, but could be even one year (Fig. 1a). Previous light-curve modeling with the usual assumption of only cool spots is thus relatively meaningless in this case. Also, the notion that the brightest magnitude

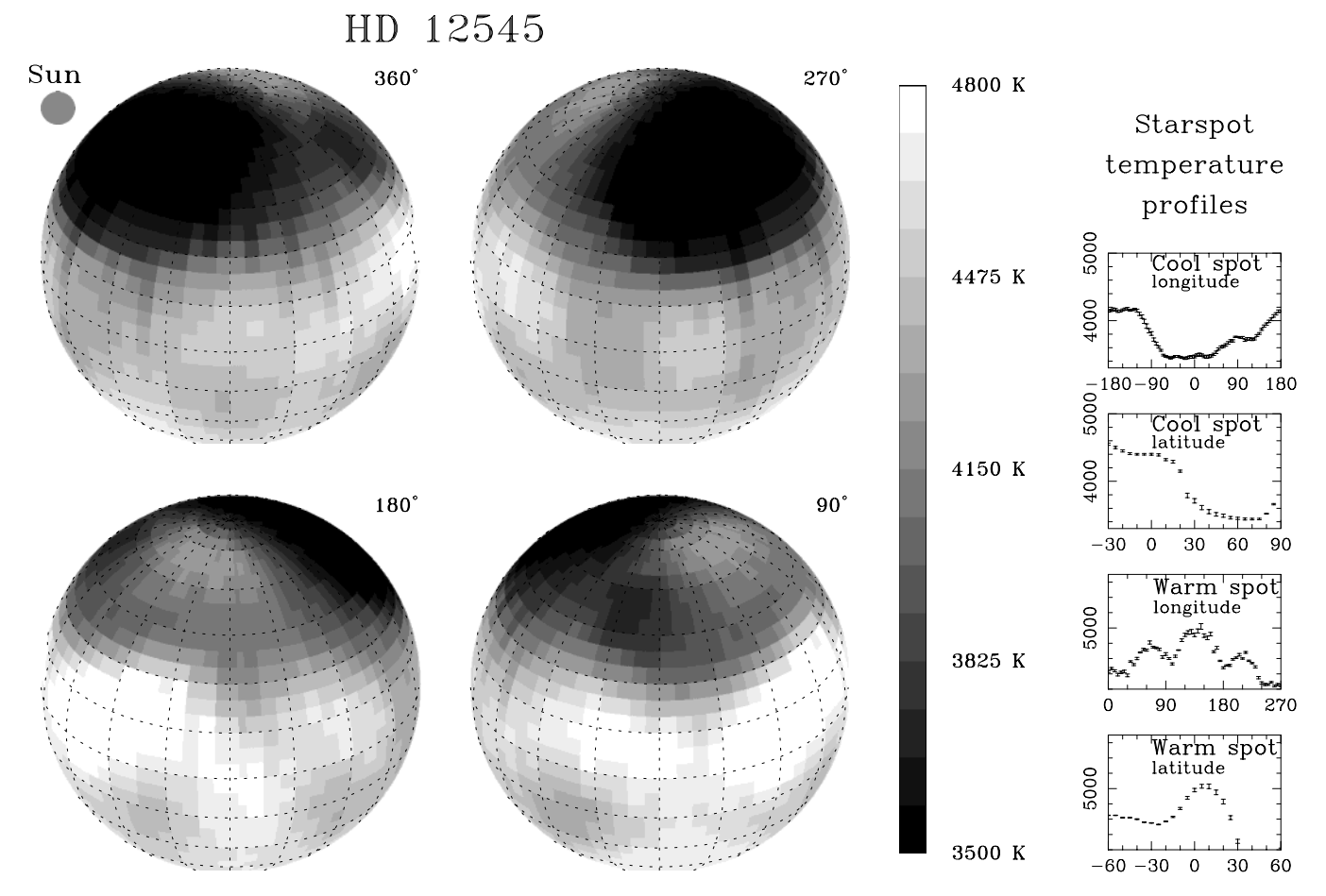


Fig. 8. Average temperature map of HD 12545 in spherical projection. The map is constructed from averaging four of the six individual maps from Fig. 5a–f. Note the comparison with the projected solar disk in the upper left corner. The small panels to the right plot the temperature profiles for the warm and cool spot along longitudinal and latitudinal cuts through their central position, respectively.

ever observed is the unspotted magnitude of the star can be severely wrong, and would produce a false areal spot coverage for HD 12545.

Our Doppler images recovered a gigantic cool starspot. With a linear extension of 12×20 solar radii, it is 60 times larger than a very large sunspot group (\approx 230,000 km as observed on Sept. 4, 1998; Schleicher & Wöhl 1998) and appears 10 times larger than the projected solar disk. Its area is thereby 10,000 times the area of the largest sunspot group. It is clearly non-symmetric with respect to the rotation axis and its central longitude is approximately 180° different to the warm spot; the cool spot is located on the hemisphere facing away from the secondary star. Because the rotation of HD 12545 is synchronized to the orbital motion, we may suspect that these spot positions are persistent active longitudes. Such an activity persistency has been found for other RS CVn binaries, e.g. for II Peg (Berdyugina et al. 1998), and could be tested with further Doppler images of HD 12545. If true, it could be interpreted as being due to a magnetic field connection with the red-dwarf secondary, which itself should be fully convective and thus harbor a magnetic field as well, and thus resembling the interacting magnetospheres originally

discussed by Uchida & Sakurai (1985) to explain the activity of RS CVn binaries.

HD 12545 is currently the star with the longest rotation period that has been mapped and shows no polar cap-like spot but an asymmetric spot craddling the pole. This might hint toward a relation with the long stellar rotation period of HD 12545 (or the low equatorial rotational velocity). A relation between the emerging latitudes of magnetic flux tubes and the stellar rotation period is predicted by the models originally put forward by Schüssler et al. (1996). For a single flux tube in a rotating star, the effect of the Coriolis force over the buoyancy force becomes smaller the longer the rotation period. The net force is then unable to deflect a magnetic flux tube off the radial rising path and toward the stellar rotation axis, which leads to predominantly mid-to-low latitude spots in case of a main-sequence star. However, if the convection zone is deep enough, as expected for a K0 giant, moderate rotation rates are already sufficient to deflect magnetic flux closer to the rotation poles.

There are still two puzzles with this scenario and HD 12545 left to be solved. First, the models of Schüssler et al. (1996) assume an equatorial-plane symmetry of the flux-tube gener-

ation and evolution. However, the polar spot on HD 12545 is large enough so that it could be detected if it had a similar counterpart on the invisible pole, but this is not obvious from our maps. Piskunov & Wehlau (1994) presented numerical simulations to detect such polar caps on the invisible pole. Although they concluded that it is currently not feasible to see the other cap, the polar spot on HD 12545 is not a symmetric cap and also reaches down to a latitude of $+30^{\circ}$ on the stellar surface, a configuration which was not included in the simulations of Piskunov & Wehlau (1994). We take this as evidence that there is no other polar counterpart on HD 12545 and speculate that the warm spot harbors a field of opposite polarity.

Second, both the warm and the large cool feature on HD 12545 are thought to be concentrations of magnetic fields originating from flux tubes that surfaced in the stellar photosphere. Their lifetimes are at least the 220 days for which we had photometry and they thus appear to be relatively long lived. Why then is the warm feature at the stellar equator while the cool feature appears close to the pole? One explanation could be that the two features were formed from fields that originated from different dynamo modes. They could be of different field strength and thus become unstable at different latitudes. A similar phenomenon is predicted for pre-main-sequence star models with a comparable ratio of radiative-core to convective-envelope dimensions as for a K giant (Granzer et al. 1999). In such a model, flux tubes at low latitudes may become unstable at low field strengths, their magnetic buoyancy is then small and their rise to the surface almost axiparallel due to the dominance of the Coriolis force. The consequence is that the flux tubes surface in two latitudinally distinct zones. On HD 12545, where the spots are so large that they fill up part of a hemisphere, the "preferred zones" are probably just the equatorial regions and the polar regions. Of course, a completely different explanation would be that such active regions are formed due to random effects of magnetoconvection near the stellar photosphere. A Zeeman-Doppler image of the surface field topology of HD 12545 could possibly resolve this issue if the star can be reobserved in a similarly favorable state of high activity. Recent advances in and applications of this technique by Donati (1999), together with the advent of 8m-class telescopes, may shed new light on the issue of stellar magnetism.

Acknowledgements. I am grateful to the Austrian Science Foundation (FWF) for their support through grant S7301-AST for the operation of the two APTs and S7302-AST for Doppler imaging. I also thank Dr. Frank Fekel (TSU-Nashville) for taking two of the KPNO spectra and Dr. Yvonne Unruh for a critical reading of the manuscript. The input of Albert " π " Washüttl's observing and data reduction skills is also highly appreciated. KPNO and its TAC are acknowledged for their continuous support of observing runs with the coudé feed telescope.

References

Berdyugina S.V., Berdyugin A.V., Ilyin I., Tuominen I., 1998, A&A 340, 437

Bidelman W.P., 1985, IAPPP Comm. 21, 53

Bopp B.W., Fekel F.C., Aufdenberg J., Dempsey R.C., Dadonas V., 1993, AJ 106, 2502

Dempsey R.C., Linsky J.L., Fleming T.A., Schmitt J.H.M.M., 1993, ApJS 86, 599

Donati J.F., 1999, MNRAS 302, 457

Dorren J.D., Guinan E.F., 1990, ApJ 348, 703

Eggen O.C., 1969, PASP 81, 553

ESA 1997, The Hipparcos and Tycho catalog, ESA SP-1200

Flower P.J., 1996, ApJ 469, 355

Granzer Th., Schüssler M., Caligari P., Strassmeier K.G., 1999, A&A, submitted

Gray D.F., 1992, The observation and analysis of stellar photospheres. Cambridge University Press, p. 243

Hampton M., Henry G.W., Eaton J.A., Nolthenius R.A., Hall D.S., 1996, PASP 108, 68

Hatzes A.P., 1993, ApJ 410, 777

Kurucz R.L., 1993, ATLAS-9, CD-ROM #13

Nolthenius R., 1991, IBVS 3589

Piskunov N.E., Kupka F., Ryabchikova T.A., Weiss W.W., Jeffrey C.S., 1995, 112, 525

Piskunov N.E., Wehlau W.H., 1990, A&A 233, 497

Piskunov N.E., Wehlau W.H., 1994, A&A 289, 868

Rice J.B., 1996, In: Strassmeier K.G., Linsky J.L. (eds.) IAU Symp. 176, Stellar Surface Structure. Kluwer, Dordrecht, p. 19

Rice J.B., Strassmeier K.G., 1998, A&A 336, 972

Rice J.B., Wehlau W.H., Khokhlova V.L., 1989, A&A 208, 179

Scarfe C.D., Batten A.H., Fletcher J.M., 1990, Publ. Dom. Astron. Obs. Victoria 18, 21

Schaller G., Schaerer D., Meynet G., Maeder A., 1992, A&AS 96, 269 Schleicher H., Wöhl H., 1998, Kiepenheuer Inst. f. Sonnenphysik, priv. commun.

Schmidt-Kaler T., 1982, In: Landolt-Börnstein, Vol. I/2b, p. 15

Schüssler M., Caligari P., Ferriz-Maz A., Solanki S.K., Stix M., 1996, A&A 314, 503

Seeds M.A., 1995, In: Henry G.W., Eaton J.A. (eds.) Robotic telescopes: current capabilities, present developments, and future prospects for automated astronomy. PASPC 79, p. 11

Strassmeier K.G., 1997, A&A 319, 535

Strassmeier K.G., Bartus J., Cutispoto G., Rodonó M., 1997a, A&AS 125, 11

Strassmeier K.G., Boyd L.J., Epand D.H., Granzer Th., 1997b, PASP 109, 697

Strassmeier K.G., Fekel F.C., Bopp B.W., Dempsey R.C., Henry G.W., 1990, ApJS 72, 191

Strassmeier K.G., Oláh K., 1992, A&A 259, 595

Strassmeier K.G., Rice J.B., 1998, A&A 330, 685

Uchida Y., Sakurai T., 1985, In: Kundu M.R., Holman G.D. (eds.) IAU Symp. 107, Unstable current systems and plasma instabilities in astrophysics. Reidel, Dordrecht, p. 281

Vogt S.S., Hatzes A.P., Misch A.A., Kürster M., 1999, ApJS, in press Vogt S.S., Penrod G.D., Hatzes A.P., 1987, ApJ 321, 496